Detached Eddy Simulation for the F-16XL Aircraft Configuration

Alaa Elmiligui[1], and Khaled Abdol-Hamid[2]
NASA Langley Research Center, Hampton, VA, 23681, USA

and

Edward B. Parlette[3]
ViGYAN, Inc., Hampton, Virginia 23666

Numerical simulations for the flow around the F-16XL configuration as a contribution to the Cranked Arrow Wing Aerodynamic Project International 2 (CAWAPI-2) have been performed. The NASA Langley Tetrahedral Unstructured Software System (TetrUSS) with its USM3D solver was used to perform the unsteady flow field simulations for the subsonic high angle-of-attack case corresponding to flight condition (FC) 25. Two approaches were utilized to capture the unsteady vortex flow over the wing of the F-16XL. The first approach was to use Unsteady Reynolds-Averaged Navier-Stokes (URANS) coupled with standard turbulence closure models. The second approach was to use Detached Eddy Simulation (DES), which creates a hybrid model that attempts to combine the most favorable elements of URANS models and Large Eddy Simulation (LES). Computed surface static pressure profiles are presented and compared with flight data. Time-averaged and instantaneous results obtained on coarse, medium and fine grids are compared with the flight data. The intent of this study is to demonstrate that the DES module within the USM3D solver can be used to provide valuable data in predicting vortex-flow physics on a complex configuration.

Nomenclature

Cp	surface pressure coefficient
L	Characteristic length, 54.16 ft
M_∞	free stream Mach number
R1&R2	grid growth parameters
Rn	Reynolds number based on reference chord
U	free stream reference velocity, ft/sec
x/c	fractional distance along the local chord, ft
y/2b	fractional distance along the wing local semispan, ft
y^+	wall normal distance
α	angle of attack, degree
δ_j	first cell height, in
ΔT	Time step

Acronyms

CAWAP	Cranked Arrow Wing Aerodynamics Program
CAWAPI	Cranked Arrow Wing Aerodynamics Program, International
DES	Detached Eddy Simulation(s)
FC	Flight Condition
kε	kε turbulence model
MSD	Modeled Stress Depletion
NATO	North Atlantic Treaty Organization

[1] Research Engineer, Configuration Aerodynamics Branch, NASA LaRC, AIAA Senior Member.
[2] Research Engineer, Configuration Aerodynamics Branch, NASA LaRC, AIAA Associate Fellow.
[3] Research Engineer, 30 Research Drive, Hampton, Virginia 23666.

RANS Reynolds-Averaged Navier-Stokes
RTO Research and Technology Organization
SA Spalart–Allmaras turbulence model
SST Shear Stress Transport turbulence mode
TA Time-Averaged
URANS Unsteady Reynolds-Averaged Navier-Stokes

I. Introduction

The Cranked Arrow Wing Aerodynamic Project International (CAWAPI) utilized the F-16XL aircraft as part of a basic research project planned in support of the High Speed Research Program (HSRP). A review of the project and how it evolved over the years is given by Lamar & Obara[1]. Flight, wind tunnel and computational studies were conducted, and various data sets were generated, analyzed, and compared to CFD results[2-13]. CAWAPI objectives were to validate new methodologies, to evaluate a number of predictive methods against available flight test data at high Reynolds numbers, and to check the technology readiness level (TRL) of Computational Fluid Dynamics (CFD) codes for a military aircraft. Military requirements result in a need for a better understanding of the aircraft characteristics before full-scale production. For this purpose, new and existing CFD codes have to be validated, and their TRL checked and/or increased. The CAWAPI-1 recommendation was to generate better grids, with improved density to capture vortical flow; to adapt to flow features; and to use higher fidelity physical models[5].

CAWAPI-2 started in 2010 as an international cooperation with contributions from several organizations. The intent was to focus on the flight conditions that CFD results from CAWAPI-1 failed to predict. In 2014, two invited AIAA special sessions were held at the 52nd AIAA Aerospace Sciences Meeting as part of the CAWAPI-2[6-13]. The objective was to find out why CFD failed to simulate FC 25 and FC 70. FC 25 is a subsonic high angle-of-attack case at flow conditions of $M_\infty = 0.242$, $\alpha = 19.84°$, and $Rn = 32.22 \times 10^6$ based on reference chord length. FC 70 is a transonic low angle-of-attack case where $M_\infty = 0.97$, $\alpha = 4.37°$, $Rn = 88.77 \times 10^6$. Relevant questions that came out of the two invited AIAA CAWAPI-2 special sessions were:

1) What is the best flow physics based model or "turbulence model" to employ?
2) Do we need to adapt for vortical flow generated at these conditions?
3) Do we have a grid converged simulation?
4) Do we have the correct geometry for the transonic case FC 70?
5) Is the flow steady or unsteady?
6) What is the effect of aero-elasticity on the solution?

As part of the CAWAPI-2 effort the authors attempted to answer the first three questions. Their results for the F-16XL configuration using the TetrUSS[14] flow analysis and CRISP CFD systems were presented in reference 13. The flow analysis was conducted for a subsonic, high angle-of-attack case FC 25, where $M_\infty = 0.242$, $\alpha = 19.84°$, $Rn = 32.22 \times 10^6$ based on the reference chord length. All the computed results were based on the assumption that the flow was fully turbulent and steady over the entire vehicle surfaces. The sensitivity of the numerical results to the Spalart-Allmaras (SA)[15], shear stress transport (SST)[16], and $k\varepsilon$[17] turbulence models was examined. Computed surface pressures were compared with corresponding flight data. In general, the $k\varepsilon$ surface Cp results compared well with the flight data, while both SA and SST gave similar results that over-predicted the data. It was observed that the accuracy of the computed surface pressure, from SA, SST and $k\varepsilon$ turbulence models, was degraded closer to the wing tip region. Surface pressures at BL 184.5 span were substantially under-predicted over most of the main wing. The reason for the discrepancy between CFD results and flight data was attributed to possible flow unsteadiness and turbulence model failure to capture vortex breakdown on the inboard wing panel. Authors surmised either a higher fidelity turbulence model or detached eddy simulation (DES) might improve the accuracy in resolving the wing tip vortex and the localized flow separation on the outer wing. The DES approach creates a hybrid model that attempts to combine the most favorable elements of URANS models and Large Eddy Simulation (LES).

In the current paper, the NASA Tetrahedral Unstructured Software System (TetrUSS)[14] flow solver USM3D is used to compute a flow field for FC 25. The present paper attempts to address first and fifth concerns in the above list. Detailed comparisons of computed surface pressures for FC 25 using Unsteady Reynolds-Averaged Navier-Stokes (URANS) and the Detached Eddy Simulation (DES) are presented and compared with flight data.

II. Computational Approach

In this section, details of the computational grids and the numerical approach that were used in the current study are presented. Various convergence criteria adopted to ensure solution convergence are also be described.

A. USM3D Flow Solver

USM3D is a tetrahedral cell-centered, finite volume, Euler and Navier-Stokes flow solver. The solver scheme allows various options for computing the inviscid flux quantities across each cell face. For the current work, Roe's flux-difference splitting (FDS) was used to compute inviscid flux and the diffusion terms were centrally differenced. Min-Mod limiter was used within the flow solver to smooth out the flow discontinuities due to shock waves. USM3D has several closure models for capturing flow turbulence effects. For the current study SA[15], kε[17] and SA-DES[18] were used. For steady simulations, the time integration will follow the implicit point Gauss-Seidel algorithm and local time stepping for convergence acceleration.

B. Unsteady Simulations and Temporal accuracy

Second-order time-stepping is an established technique for improving the time-accuracy of conventional numerical schemes for unsteady flow computations. This strategy requires storing solution information at prior time levels and performing a sub-iteration of the solution between time steps to synchronize all cell properties at the next time level[19]. Two second-order time-stepping schemes were used in the current study. The first option is a second-order time-accurate scheme based on three-point backward differencing and pseudo time variable, and will be referred to later in the paper as Option-1. The second approach is a second-order time-accurate scheme based on three-point backward differencing and Newton's method, and will be referred to later in the paper as Option-2. The first scheme is the most stable of the currently available time-accurate methods in USM3D. However, it requires a large number of sub-iterations and can be quite costly to use. The second approach is more efficient than the pseudo-time method as it converges faster at each physical time step[19]. For the current set of simulations, 10 sub-iterations per time-step were used, which was adequate to obtain at least 2.5 orders of magnitude reduction in the residuals of the governing equations. Comparison between the results from the two time stepping schemes is presented in the results and discussions section.

USM3D non-dimensional time step for the temporally second order time-accurate computations was computed as:

$$\Delta t = L/(Mach*N)$$

where L is a representative characteristic length and N is the number of time steps to traverse characteristic length, L. In the current study, vehicle length of 54.16 ft was taken as the characteristic length. Four non-dimensional time steps, Δt =1, 2, 5, and 10, were used corresponding to a physical time step of 0.05, 0.1, 0.25, and, 0.5 sec, respectively. Number of time steps to traverse vehicle length varied between 270 and 2700 iterations. Computations using all four time steps are presented and compared to flight data in the results and discussions section. Most of the presented results are computed with Δt = 5 corresponding to N = 540.

C. Turbulence Modeling

For the unsteady flow simulations of FC 25, URANS was coupled with the standard turbulence closure models, (kε and SA). Flow solvers based on the URANS equations with standard turbulence closure models might not be adequate to account for the entire spectrum of turbulent motions. Unsteady geometry dependency and three dimensional turbulent eddies are the main characteristics of massively separated flows. However, URANS turbulence models prematurely diffuse them. The full direct numerical simulation of both geometry-based and eddy-based separations on complex configurations is prohibitively expensive with current computer technology. An innovative interim solution to this shortcoming was proposed in reference 17 called Detached Eddy Simulation (DES) and is implemented in USM3D via a simple modification to the SA turbulence model[15]. The DES approach creates a hybrid model that attempts to combine the most favorable elements of URANS models and Large Eddy Simulation (LES). The standard SA model contains a wall-distance based destruction term to reduce the turbulent viscosity in the laminar sub layer and the log layer. By a simple modification of the wall distance parameter away from the surface to reflect the local cell size in the field, the near-surface properties of the URANS model can be preserved while transitioning to an LES model away from the surface. Computed surface pressures using RANS, URANS and DES for FC 25 will be presented in the results and discussions section.

D. Grid Generation

The present results utilized the grids from reference 13 where they assumed that the F-16XL flow field is symmetric. Based on this assumption, the grids were generated on half the airplane. This set of grids will be referred to later in the paper as Grid-1. The surface triangulations along with the field tetrahedral volume grids were generated using GRIDTOOL and VGRID software. A rectangular box that encompasses the vehicle is typically used to define the computational domain far-field boundaries. Each face of this rectangular box is located several body lengths away from the configuration in the upstream, radial and downstream direction. The far field boundaries were located at 100 times the mean aerodynamic chord of the wing. As a general practice, each final converged solution is analyzed to insure that the laminar sub-layer has been grid resolved and that the average y^+ is less than 1.

Three different grids (coarse, medium, and fine) have been used to facilitate grid effects in the results using the different approaches. The guidelines established by the Drag Prediction Workshop[20] and the High Lift Prediction Workshop[21] to address solution sensitivity to grid refinement, were adopted in the grid generation. Figure 1 shows the representative computational grids on the surface and the near-field view for typical cross sectional cuts of the coarse, medium, and fine grid. There were 15 components, with different sizes and shapes over the F-16XL configuration. Such geometrical complexity presented a challenge for the grid generation and the flow solver to properly capture the associated flow physics and the resulting aerodynamic properties of the vehicle. Table 1 below provides the values of δ_1, the total number of cells in the viscous layer, and the total number of surface elements for different grids. A factor of 2/3 was used to size the value of δ_1, for each consecutive grid refinement. Furthermore, a factor of 1.26 was used to construct the viscous layers (δj) in the radial direction by setting the grid growth rate parameters R1 =1.16 and R2 = 0.04 for all the grids used in the present investigation.

$$\delta_j = \delta_1 \, (1+R1(1+R2)^{j-1})^{j-1}$$

In this equation, the variable δ_1 is the first cell height next to the solid surface in the normal direction. This grid system is suitable for cell-centered flow solvers.

Table 1 provides the average normal spacing to viscous wall in terms of $y+$ coordinate, and the values of the first cell height δ_j for the list of grids. The DES grids covered the full airplane to simulate any three-dimensional turbulence effects on the flow. This was achieved by mirroring reference 13 grids around the XZ-plane. The DES set of grids will be referred to later in the paper as Grid-2. A second set of DES was also performed on Grid-1. Comparison between DES results from Grid-1 and Grid-2 are presented and discussed in the results and discussions section.

Table 1: Grids and computational resources.

Grid	Number of Cells Grid-1	Number of Cells, DES Grid-2	First cell height, δ_1, in	y+ average
Coarse	19,370,847	38,741,694	0.00092	1.108
Medium	62,473,588	124,947,176	0.00061	0.757
Fine	143,034,292	286,068,584	0.00041	0.516

E. Solution Development and Convergence

All calculations were made using Roe's flux difference splitting method. Three sets of results are presented in the results and discussions section:

- RANS simulations coupled with the SA and kε turbulence models from reference 13. (Grid-1)
- URANS simulations coupled with SA and kε turbulence models. (Grid-2)
- DES (Grid-1 or Grid-2)

In general, solution convergence was evaluated by monitoring variations in all six longitudinal and lateral force and moment aerodynamic coefficients. A solution was considered converged when fluctuations in these coefficients are reduced to less than 0.5% of their respective average values calculated over the previous 2000 iterations. The NAS supercomputer was used to compute all of the cases. A typical case completes in less than 12 hours.

III. Results and Discussions

The subsonic high angle-of-attack FC 25 was simulated for the flow around the F-16XL. Computational results, surface static pressures, are presented and compared with flight data. F-16XL FC 25 computations were performed at a free stream Mach number of 0.242, an angle of attack of 19.4 degrees, and Reynolds number equal to 32.22 x 10^6 based on reference chord length. Vortical-flow phenomena over the upper surface of the wing are expected. The F-

16XL has a cranked leading edge sweep angles of 70° sweep for the inboard wing panel and 50° sweep for the outboard wing panel.

The F-16XL USM3D surface pressure distribution is shown in Fig. 2a for typical flow simulation. The flow structure consists of several vortices: i) an inboard vortex originating from the wing apex, ii) an outboard primary vortex originating from the wing leading edge outboard of the crank, and iii) an airdam vortex. Figure 2b shows the surface streamlines. The convergence-divergence of the surface streamlines show the location of the flow separation and reattachment. Figures 2a and 2b show the footprint of the outer-wing primary vortex forming at the crank and traveling downstream and outboard towards the tip and the missile store. Flight data were extracted at different fuselage stations (FS) and butt line (BL) cuts. Computed surface pressures were extracted at various FS and BL locations for comparison with flight test data. The black lines in Fig. 2c show the seven FS locations, 185, 300, 337.5, 375, 407.5, 450 and 492.5. Figure 2d shows the seven BL locations: 55, 70, 80, 95, 105, 153.5 and 184.5. BL 184.5 is highlighted in red as it presented the greatest challenge for the turbulence models to predict, reference 13. The primary vortex starts at FS 185 and the secondary vortex starts at around FS 407.5. There are strong interactions in the vortex system over the F-16XL. The inner-wing secondary vortex strikes the airdam followed by an airdam vortex emanating downstream. The vortex wake off the missile fins, at the vicinity of BL 184.5, makes the flow even more complex and unsteady.

Reference 13 performed solution verification for FC 25 using formal grid refinement studies, the solution of error transport equations, and adaptive mesh refinement. It was observed that surface pressures at BL 70, BL 105, and FS 300 show little effect of grid refinement. At these three stations, coarse, medium and fine grid surface pressures are almost identical and grid convergence was achieved. In general, all computed results were in good agreement with the measured data. The kε turbulence model provided the better comparisons with upper surface pressure data than the SA turbulence model results. Grid resolution effects were observed further outboard on the main wing at station BL 184.5. Even fine grid surface pressures did not agree with the measured surface pressures at this station and grid convergence was not achieved. The reason for the discrepancy might be due to turbulence model failure to predict vortex break down and the onset of separation on the outer wing. In the present study, flow field was simulated using URANS coupled with standard turbulence closure models as well as the one-equation Detached Eddy Simulation (DES) model of Spalart. In the following sections, we demonstrate the effects of URANS, DES, and grid refinement on predicting the flow field around an F-16XL.

A. URANS Simulations with Standard Turbulence Closure Models.

In an attempt to capture unsteadiness at BL 184.5, USM3D was first run in an unsteady mode coupled with standard turbulence closure models (kε and SA). Figure 3 shows comparisons of the steady and unsteady RANS coupled with the kε turbulence model for FC 25. The RANS solution was conducted on Grid-1 while URANS utilized Grid-2. The time averaged URANS solution as well as instantaneous surface pressures at different time iterations are also shown in Figure 3. Overall good agreement was observed between RANS, URANS and flight data at FS 300 as shown in Figure 3a. The URANS simulation is identical to the steady RANS solution and both agreed with flight data at this location where flow is steady. However, both schemes failed to predict unsteadiness in the flow field as shown in Fig. 3b. Fig. 4 shows that the SA turbulence model showed similar behavior with no indication of unsteadiness in the flow field. USM3D URANS simulations of FC 25, using standard turbulence closure models, failed to predict unsteadiness at BL 184.5 and were not adequate to account for the entire spectrum of turbulent motions. URANS failed to predict the complex flow pattern in the vicinity of the wing tip.

The authors considered DES as the next option in resolving the complex flow pattern in order to improve the accuracy in resolving the wing tip vortex and the localized flow separation on the outer panel of the wing. The DES approach creates a hybrid model that attempts to combine the most favorable elements of URANS models and LES and was considered by the authors as a good candidate to capture the complex flow pattern at the outer wing.

B. Dettached Eddy Simulation

DES were conducted for the subsonic, high angle-of-attack case, FC 25, where $M_\infty = 0.242$, $\alpha = 19.84°$, Rn = 32.22 x 10^6 based on the reference chord length. Simulations were conducted on all three grid levels using second-order time-stepping Option-1 and Option-2 schemes. Ten sub-iterations were used in all the computations conducted in this study.

To investigate the sensitivity of DES to the time step, four non-dimensional time steps, Δt =1, 2, 5, and 10, were used on the coarse grid for the Grid-2 family. Computer resources are reduced with the increase of Δt. Fig. 5 shows the effect of time step on the computed results using Option-1. The predictions are almost identical between all four non-dimensional time steps for most of the stations. Time averaged (TA) DES are time step converged, however, Fig. 5c shows that BL 153.5 is the only station where results for Δt of 5 and 10 deviated from the results of the smaller Δts.

Either increasing the number of sub-iterations for Δt greater than 5 or using Δt less than 2 using Option-1 time step is needed to achieve grid convergence at BL 153.5.

Fig. 6 shows the effect of time step on the computed results using Option-2. The predictions are almost identical between all four non-dimensional time steps for all stations. TA DES are time step converged even at BL 153.5. This is the station where DES using Option-1 showed slower convergence; i.e., Δts less than 10, can be used for FC 25 F-16XL DES using Option-2.

Fig. 7 shows comparisons between flight data and DES using both time stepping schemes using Δt = 1. The black line in Fig. 7 is RANS kε solution while the red line is DES using Option-1 and the blue line is DES using Option-2. In general, overall there is good agreement between the two time stepping schemes and the flight data. Figure 9b shows that DES resolved the leading edge vortex better than the RANS kε model. Fig. 7c shows that Option-1 fell short of capturing the magnitude of the peak at x/c = 0.1333. Fig. 7d shows that both time stepping schemes captured unsteadiness in the flow at BL 184.5 better than the kε RANS solution, which failed to capture the unsteadiness. All DES results shown subsequently will use Option-2 with Δt of 5.

A DES grid convergence study was conducted. The size of the coarse, medium, and fine grid are reported in Table 1. Simulations were conducted on all grid levels using Grid-2. Figure 8 shows comparisons of DES on the coarse, medium and fine grids for FC 25. Figure 8 shows that solution is grid converged except at FS 185, where DES on the 38 million cell, coarse grid, differs from the DES on the medium and fine grids. Authors are currently investigating reasons for the discrepancy at FS 185 and expect that the grid at FS 185 might be suffering Modeled Stress Depletion (MSD), as discussed in detail in reference 22. MSD occurs when the grid is gradually refined or when a boundary layer thickens and nears separation. Authors surmise that Delayed DES could remedy such behavior as recommended by reference 22. Figure 8a, BL 55, shows that DES fine solution accurately captured the peak at x/c ≈ 0.1. Based on this DES grid convergence study, the medium grid will be used for the rest of the paper.

Figure 9 shows comparisons of flight data, RANS kε and SA turbulence models results with DES on the medium grid. The DES results utilizing Grid-2 are in good agreement with flight data. DES was able to better capture surface pressure distribution at BL 184.5, Fig 9d. This is the station that presented the greatest challenge for the steady RANS and URANS kε and SA turbulence model simulations.

Fig. 10 shows comparison between DES time averaged (TA) results and snapshots of DES at different time levels. The black line in Fig. 10 is the time averaged DES results while colored lines represent snapshots of DES at different time steps. DES results at BL 70 (Fig. 10a) show that flow is steady, and that the TA DES results and the DES snapshots results are identical. The on start of flow unsteadiness can be seen at BL 95 (Fig. 10b) where DES results at different time levels fluctuate around flight data and TA DES results. The flow on the outer wing shows a high level of unsteadiness as shown at BL 153.5 (Fig. 10c) and BL 184.5 (Fig. 10d). The reason of the unsteadiness is attributed to the vortices on the wing upper surface.

Figure 11 shows the vortex structure superimposed on the surface pressure for DES of FC 25 using the medium grid from Grid-2 and Option-2 with Δt of 5. The unsteadiness in the flow can be seen by comparing that the non-symmetry of the formation of the primary and secondary vortices on the left and right wings.

For DES using Grid-2, the flow was originally assumed to be non-symmetric. A second set of DES was also conducted on Grid-1 to compare with Grid-2 results. Figure 12 shows the effect of running DES on Grid-1 and Grid-2. Overall DES on Grid-1 with symmetry BC generally matched DES results on Grid-2, full airplane grid. However, Grid-1 results slightly deviate from Grid-2 at FS 337.5, 375 and 407.5 as shown in Fig. 12d-f. Running on Grid-1 reduces computer resources by half as compared to running on Grid-2 for the full airplane.

In general, URANS failed to predict unsteadiness over the outboard wing panel and was very similar to RANS results. However, the DES results showed that the flow on the outer wing is unsteady. The time-averaged DES surface pressure data matched flight data better than either URANS or RANS results. The DES was able to resolve the wing tip vortex and the localized flow separation on the outer panel of the F-16XL wing

IV. Concluding Remarks

Numerical simulations of the flow around an F-16XL were performed as a contribution to the CAWAPI -2 using the USM3D CFD code. Unsteady flow simulations were computed for a freestream Mach number of 0.242, an angle of attack of 19.4 degrees, and a Reynolds number equal to 32.22 x 10^6 based on reference chord length to match FC 25 i.e., the low speed high angle-of-attack case.

URANS coupled with standard turbulence closure models, and DES were utilized to capture the unsteady vortex flow over the wing of the F-16XL. URANS and DES time-averaged and instantaneous surface static pressure profiles were extracted and compared with flight data. A second-order time-accurate scheme based on

three-point backward differencing and pseudo time variable (Option-1), and a second-order time-accurate scheme based on three-point backward differencing and Newton's method (Option-2) were used in the simulations. Ten sub-iterations were used in all the computations conducted in this study that insured 2.5 orders of magnitude in convergence for time step (Δt) range of 1-10. Results showed that the Option-2 method gave better and consistent results with varying time step range of 1-10.

URANS failed to predict unsteadiness over the outboard wing panel that is similar to the RANS results. On the other hand, the DES results showed that the flow on the outer wing is unsteady. The reason for the unsteadiness is attributed to the primary and secondary vortices that formed on the wing upper surface. The time-averaged DES surface pressure data matched flight data better than either URANS or RANS results. The DES was able to resolve the wing tip vortex and the localized flow separation on the outer panel of the F-16XL wing.

Two sets of grid families were generated; one modeling half the airplane (Grid-1) that uses a symmetry boundary condition, and the second modeling the full configuration (Grid-2). Overall DES on Grid-1 generally matched DES results on Grid-2. For each set of grid families, coarse, medium, and fine grids was generated to facilitate the grid convergence study. Running on Grid-1 reduces computer resources by half in comparison with Grid-2. The DES grid convergence study showed that the DES was grid converged except at a location of FS 185 using fine grid, where it is believed that DES might be suffering from Modeled Stress Depletion. Authors surmise that Delayed DES could remedy such behavior. Future work by the authors will involve adding Delayed DES to USM3D solver and recalculating F-16XL FC 25.

References

[1] Obara, C. J., and Lamar, J. E., "Overview of the Cranked-Arrow Wing Aerodynamics Project International," Journal of Aircraft, Vol. 46, No. 2, 2009, pp. 355–368.

[2] Lamar, J. E., Obara, C. J., Fisher, B. D., and Fisher, D. F., "Flight, Wind-Tunnel, and Computational Fluid Dynamics Comparison for Cranked Arrow Wing (F-16XL-1) at Subsonic and Transonic Speeds," NASA TP 2001-210629, Feb. 2001.

[3] Boelens, O. J., Badcock, K. J., Elmilgui, A., Abdol-Hamid, K. S., and Massey, S. J., "Comparison of Measured and Block Structured Simulations for the F-16XL Aircraft," Journal of Aircraft, Vol. 46, No. 2, 2009, pp. 377–384.

[4] Görtz, S., Jirásek, A., Morton, S. A., McDaniel, D. R., Cummings, R. M., Lamar, J. E., and Abdol-Hamid, K. S., "Standard Unstructured Grid Solutions for CAWAPI F-16XL," Journal of Aircraft, Vol. 46, No. 2, 2009, pp. 385–408.

[5] Rizzi, A., Jirásek, A., Lamar, J. E., Crippa, S., Badcock, K. J., Boelens, O. J., "Lessons Learned from Numerical Simulations of the F-16XL Aircraft at Flight Conditions," Journal of Aircraft, Vol. 46, No. 2, 2009, pp. 423–441.

[6] James M. Luckring; Arthur W. Rizzi, "Toward Improved CFD Predictions of Slender Airframe Aerodynamics Using the F-16XL Aircraft (CAWAPI-2)", AIAA 2014-0419 presented at the 52nd AIAA Aerospace Sciences Meeting, National Harbor, Maryland, January 13–17, 2014.

[7] Maximilian M. Tomac; Adam Jirasek; Arthur W. Rizzi, "Factors Influencing Accurate Shock Vortex Interaction Prediction on F-16XL Aircraft", AIAA 2014-0420 presented at the 52nd AIAA Aerospace Sciences Meeting, National Harbor, Maryland, January 13–17, 2014.

[8] Adam Jirasek; Luca Cavagna; Luca Riccobene; Sergio Ricci; Arthur W. Rizzi, "Aeroelastic Analysis of the CAWAPI F-16XL Configuration at Transonic Speeds", AIAA 2014-0421 presented at the 52nd AIAA Aerospace Sciences Meeting, National Harbor, Maryland, January 13–17, 2014.

[9] Adam Jirasek; Maximilian M. Tomac; Arthur W. Rizzi, "Improved Predictions for high Angle of Attack Flow around the F-16XL Aircraft", AIAA 2014-0422 presented at the 52nd AIAA Aerospace Sciences Meeting, National Harbor, Maryland, January 13–17, 2014.

[10] Okko J. Boelens; James M. Luckring, "Flow Analysis of the F-16XL Aircraft (CAWAPI-2) At Transonic Flow Conditions", AIAA 2014-0757 presented at the 52nd AIAA Aerospace Sciences Meeting, National Harbor, Maryland, January 13–17, 2014.

[11] Stephan M. Hitzel, "Vortex Flows of the F-16XL Configuration - CAWAPI-2 Free-Flight Simulations", AIAA 2014-0758 presented at the 52nd AIAA Aerospace Sciences Meeting, National Harbor, Maryland, January 13–17, 2014.

[12] Arthur W. Rizzi ,"What was Learned in Predicting Slender Airframe Aerodynamics with the F-16XL Aircraft", AIAA 2014-0759 presented at the 52nd AIAA Aerospace Sciences Meeting, National Harbor, Maryland, January 13–17, 2014.

[13] Alaa A. Elmiligui, Khaled S. Abdol-Hamid, Peter A. Cavallo, and Edward B. Parlette, "USM3D Numerical Simulations For the F-16XL Aircraft Configuration", AIAA 2014-0756 presented at the 52nd AIAA Aerospace Sciences Meeting, National Harbor, Maryland, January 13–17, 2014.

[14] TetrUSS Web page: http://tetruss.larc.nasa.gov/usm3d/index.html, May 201

[15] Spalart, P. R., Allmaras, S.R.: A One-Equation Turbulence Model for Aerodynamic Flows. AIAA Paper No. 1992-0439.

[16] Menter, F. R., "Improved Two-Equation k-omega Turbulence Models for Aerodynamic Flows", NASA TM103975, October 1992.

[17] Jones, W. P., and Launder, B. E., "The Prediction of Laminarization With a Two-Equation Model of Turbulence," Int. J. Heat & Mass Transf., vol. 15, no. 2, Feb. 1972, pp. 301-314

[18] Spalart, P.R., Jou, W-H., Strelets, M., and Allmaras, S.R., "Comments on the Feasibility of LES for Wings, and on a Hybrid RANS/LES Approach, Advances in DNS/LES," 1st AFOSR International Conference on DNS/LES, Greyden Press, Columbus, OH, 1997.

[19] Mohagna Pandya, Neal Frink, Khaled Abdol-Hamid, and James Chung., "Recent Enhancements to USM3D Unstructured Flow Solver for Unsteady Flows", AIAA 2004-5201

[20] 5th AIAA CFD Drag Prediction Workshop, AIAA, New Orleans, LA, http://aaac.larc.nasa.gov/tsab/cfdlarc/aiaa-dpw// [retrieved 21 November 2013].

[21] 2nd AIAA CFD High Lift Prediction Workshop (HiLiftPW-2), AIAA, San Diego, CA, http://hiliftpw.larc.nasa.gov/ [retrieved 21 November 2013].

[22] Spalart, P. R., Deck, S., Shur, M. L., Squires, K. D., Strelets, M. Kh. , Travin, A., "A new version of detached-eddy simulation, resistant to ambiguous grid densities", Journal of Theoretical and Computational Fluid Dynamics, (2006) 20: 181–195.

a) Surface Coarse Grid **b) Surface Medium Grid** **c) Surface Fine Grid**

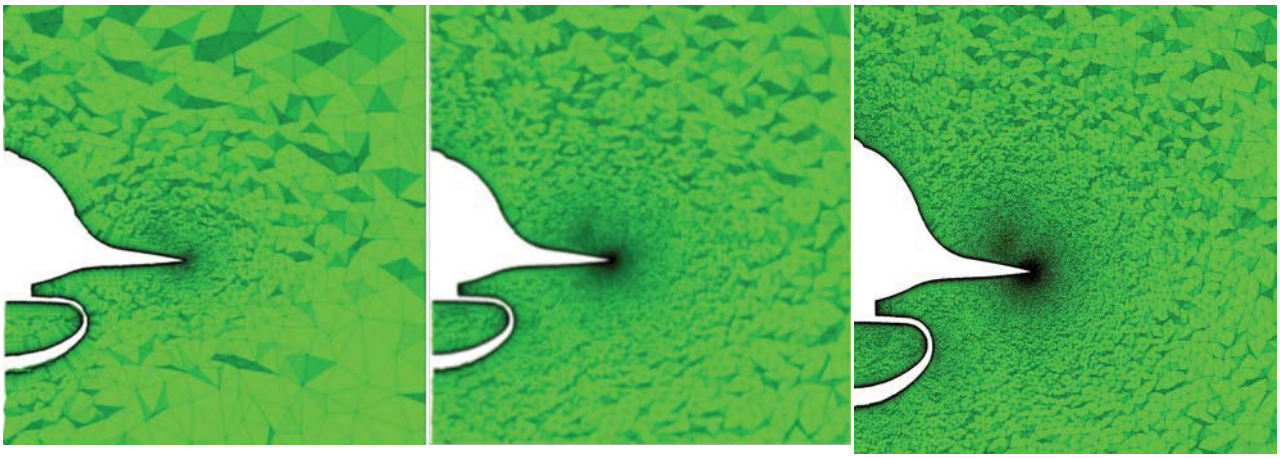

d) FS = **185 Coarse Grid** **e)** FS = **185 Medium Grid** **f)** FS = **185 Fine Grid**

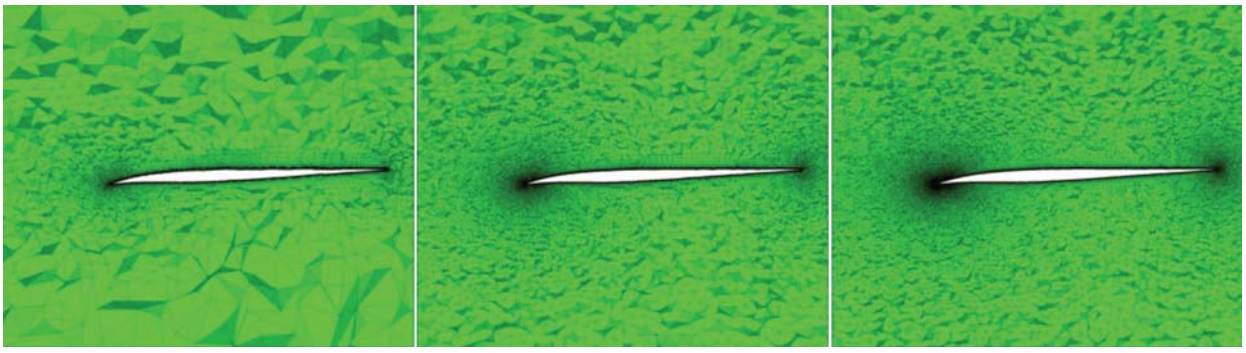

g) BL =**184.5 Coarse Grid** **h)** BL =**184.5 Medium Grid** **i)** BL =**184.5 Fine Grid**

Figure 1. Computational grid distribution on the surface and at FS 185 and BL 184.5 for the coarse, medium, and fine grids.

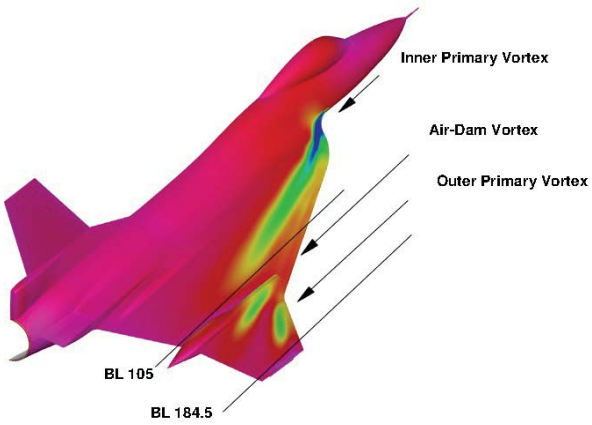

a) Surface pressure distribution

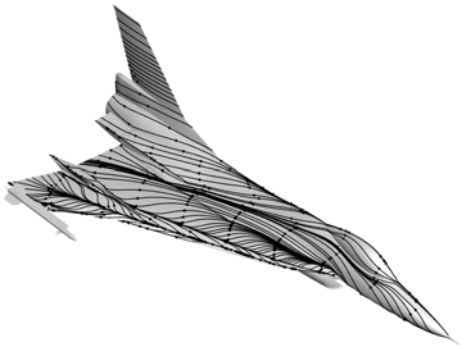

b) Surface streamlines

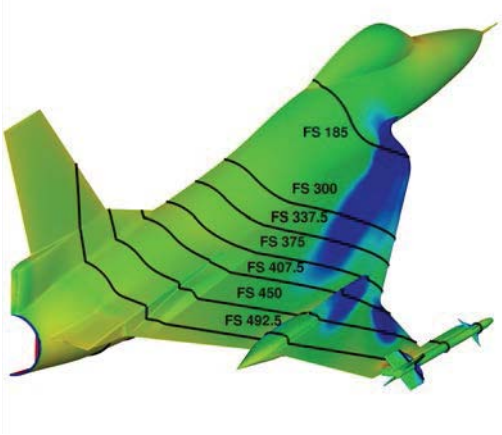

c) Fuselage stations

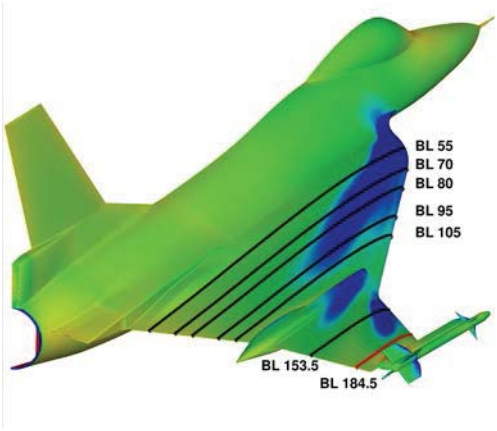

d) Butt lines

Figure 2. USM3D solution of the F-16XL at M_∞ = 0.242, α = 19.84°, and Rn = 32.2x10^6.

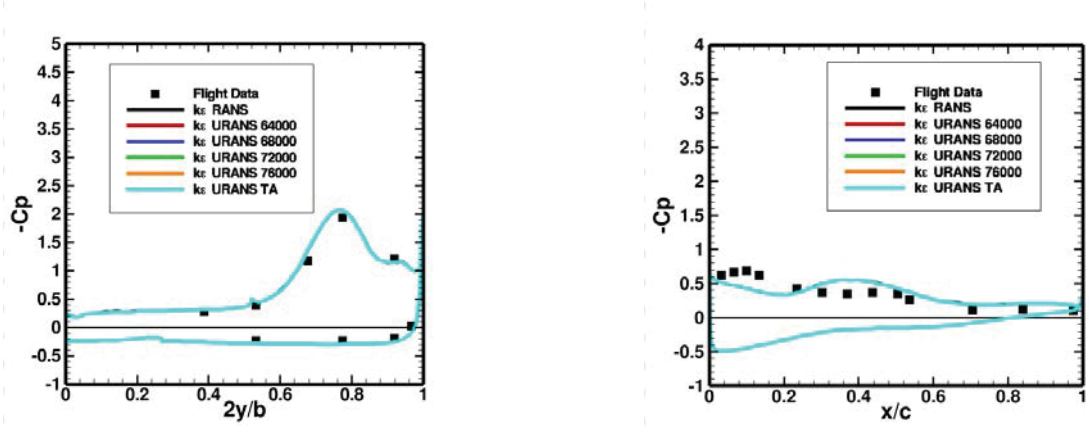

(a) FS 300 **(b) BL 184.5**

Figure 3. Comparison of flight data surface pressure distributions, with RANS, and URANS snapshot and time averaged results on the coarse grid, (Grid-2).
(M_∞ = 0.242, α = 19.84°, Rn = 32.2 X 10^6, kε turbulence model)

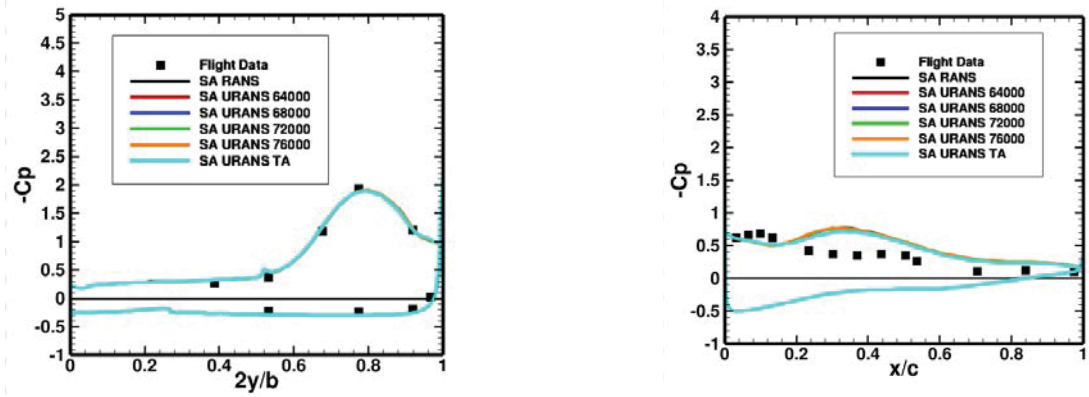

(a) FS 300 **(b) BL 184.5**

Figure 4. Comparison of flight data surface pressure distributions, with RANS, and URANS snapshot and time averaged results on the coarse grid, (Grid-2).
(M_∞ = 0.242, α = 19.84°, Rn = 32.2 X 10^6, SA turbulence model)

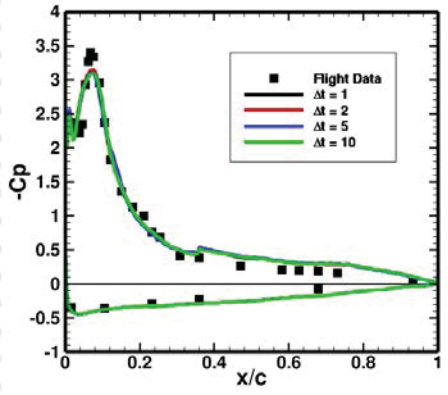

(a) BL 55

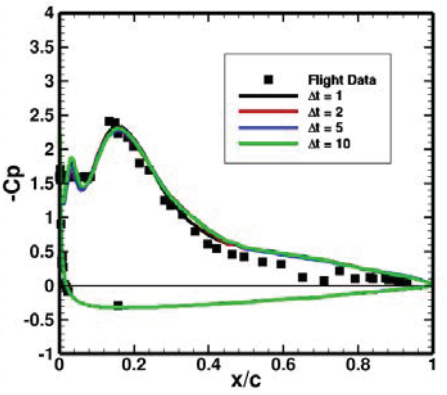

(b) BL 70

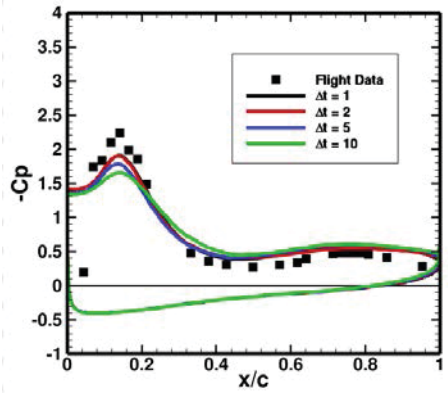

(c) BL 153.5

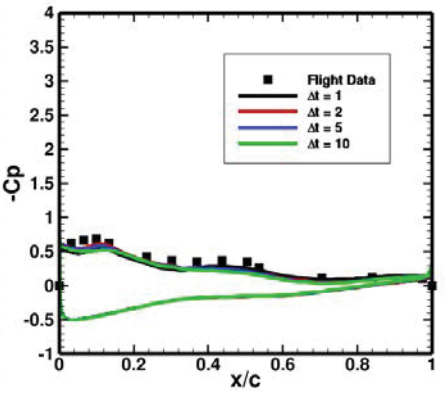

(d) BL 184.5

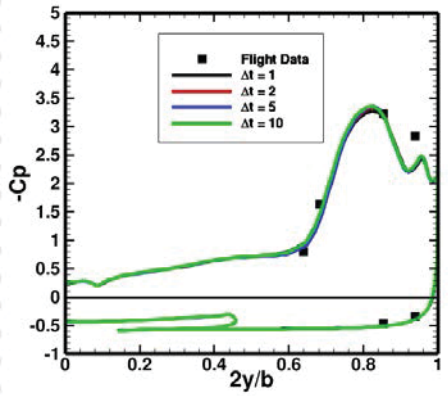

(e) FS 185

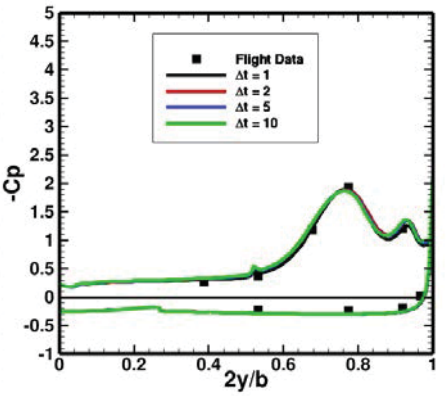

(f) FS 300

Figure 5. Effect of time step on DES time averaged surface pressure results using Option-1, (M_∞ = 0.242, α = 19.84°, Rn = 32.2 X 10^6).

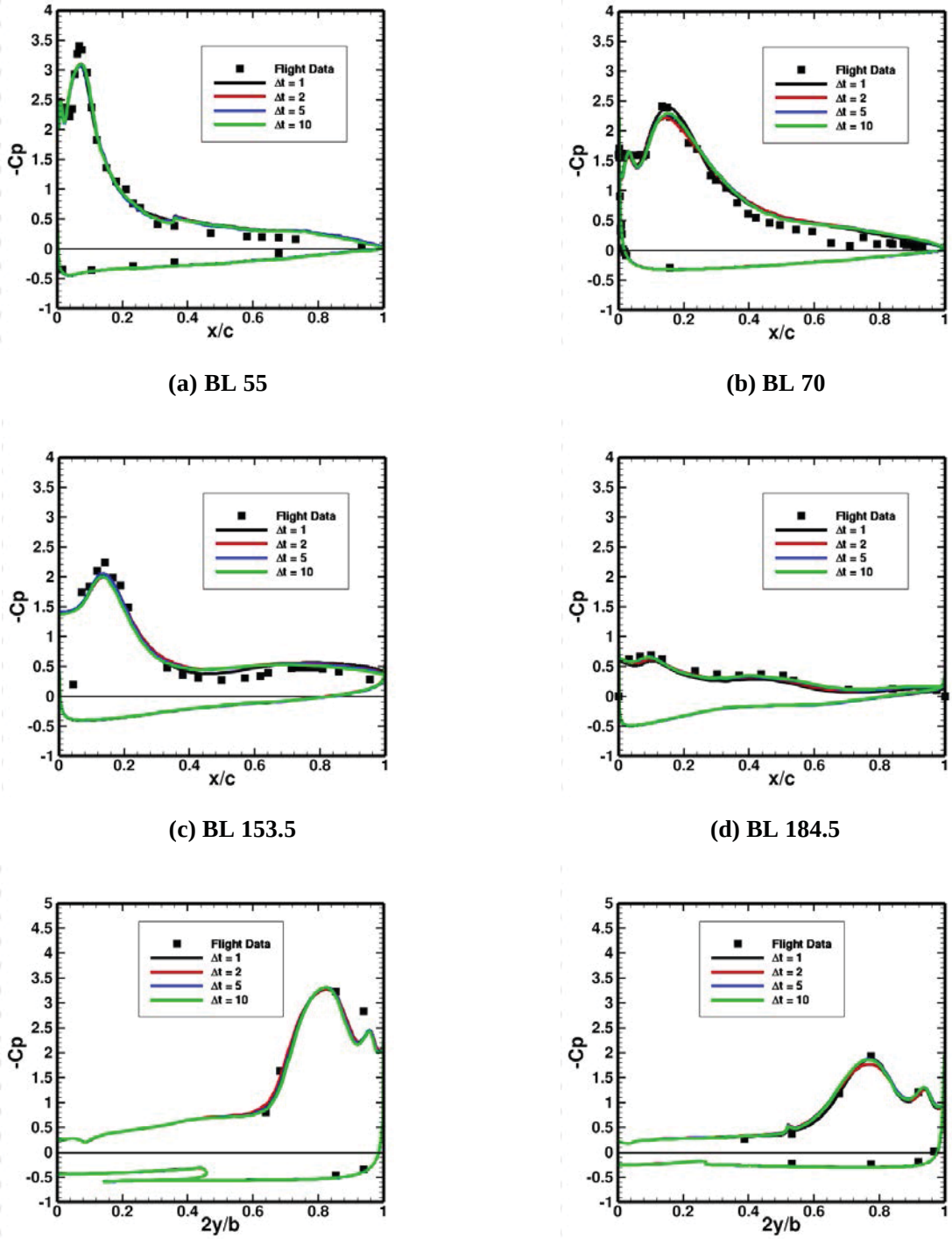

(a) BL 55 **(b) BL 70**

(c) BL 153.5 **(d) BL 184.5**

(e) FS 185 **(f) FS 300**

Figure 6. Effect of time step on DES time averaged surface pressure results using Option-2, (M_∞ = 0.242, α = 19.84°, Rn = 32.2 X 10^6).

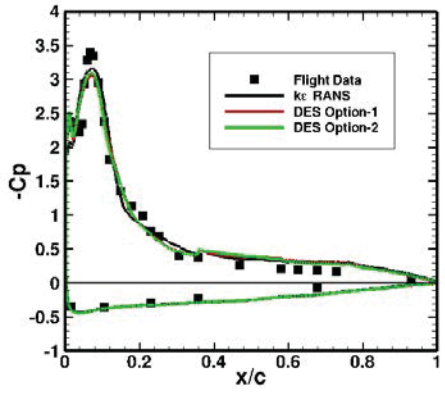

(b) BL 55

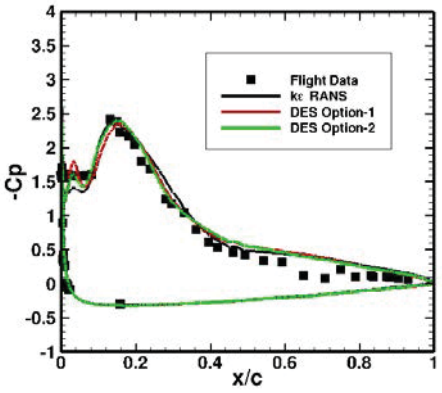

(b) BL 70

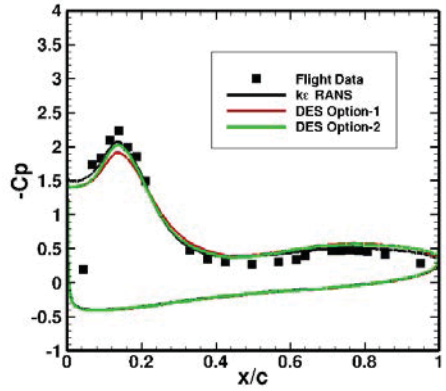

(c) BL 153.5

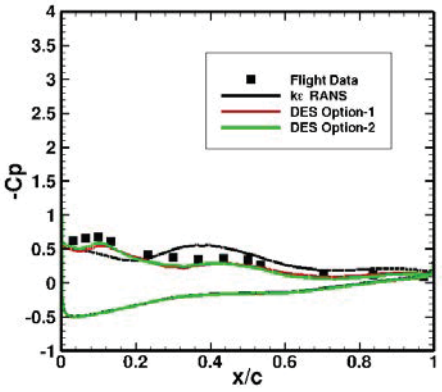

(d) BL 184.5

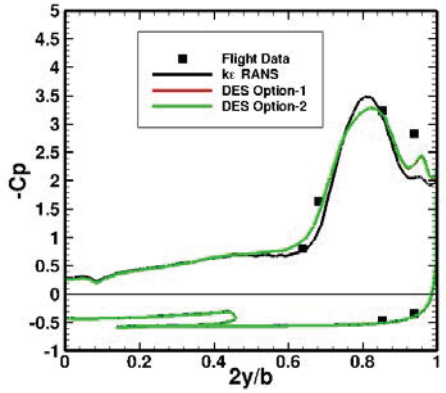

(e) FS 185

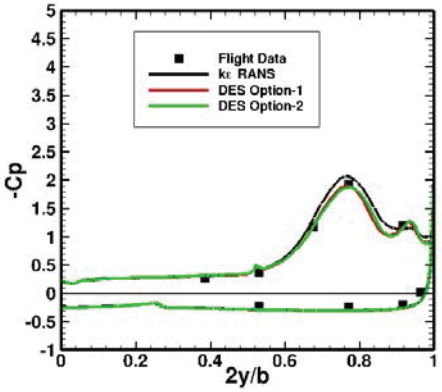

(f) FS 300

Figure 7. Comparison between DES time averaged surface pressure results using Option-1 and Option-2, (M_∞ = 0.242, α = 19.84°, Rn = 32.2 X 10^6).

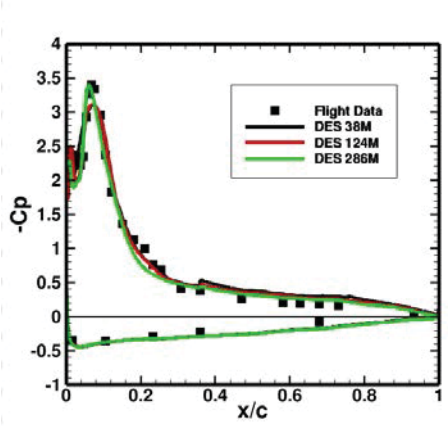

(a) BL 55

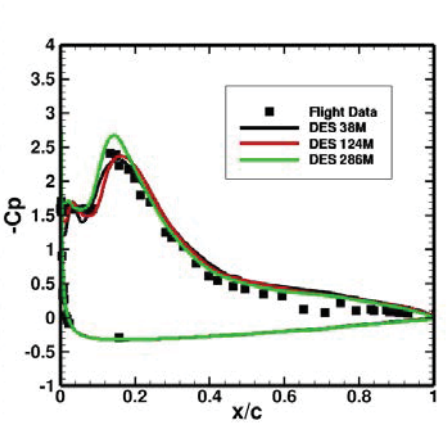

(b) BL 70

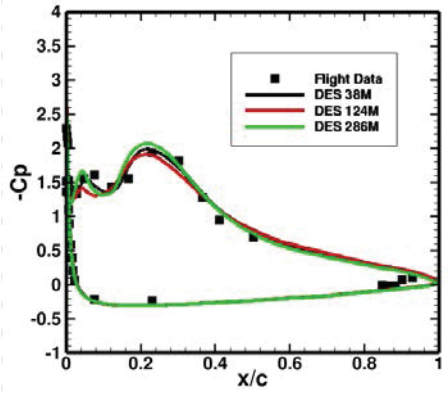

(c) BL 80

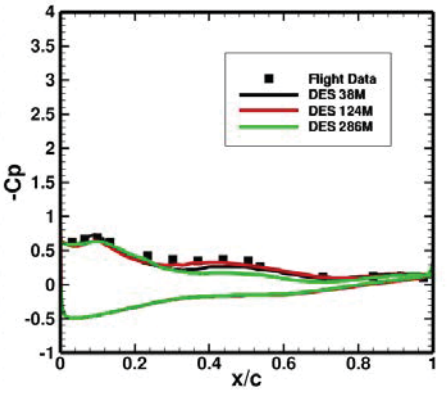

(d) BL 184.5

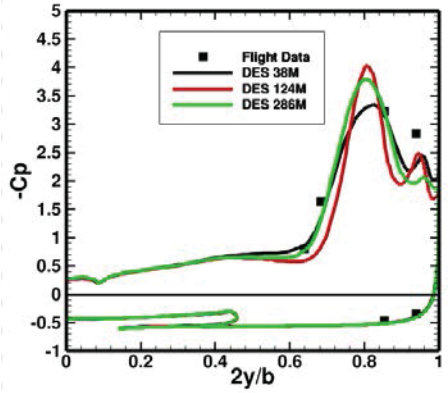

(e) FS 185

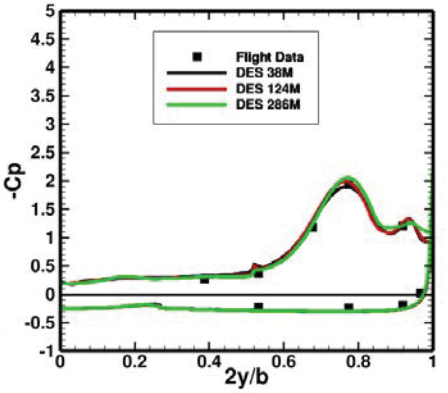

(f) FS 300

Figure 8. Surface pressure distributions of flight data and time averaged results from DES on coarse, medium and fine Grids, (Grid-2).
(M_∞ = 0.242, α = 19.84°, Rn = 32.2 X 10^6).

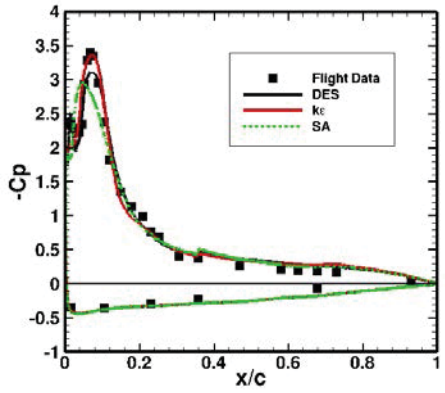

(a) BL 55

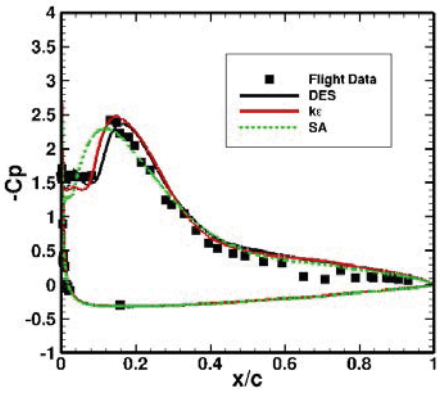

(b) BL 70

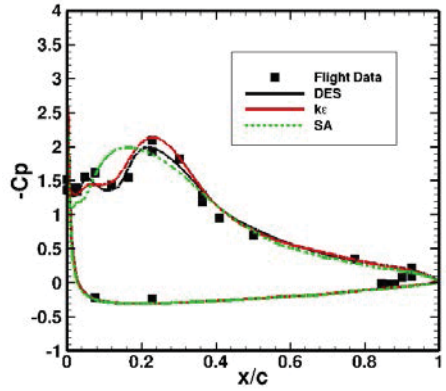

(c) BL 80

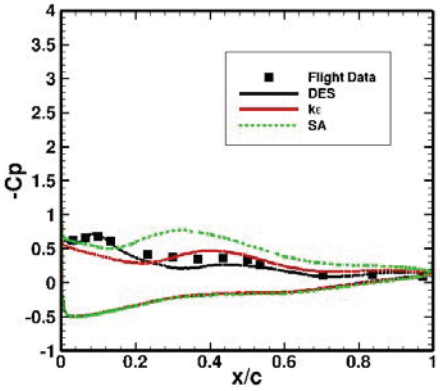

(d) BL 184.5

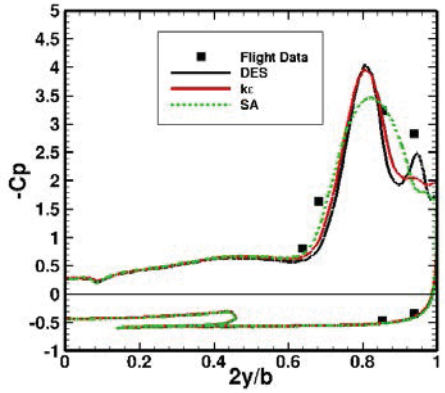

(e) FS 185

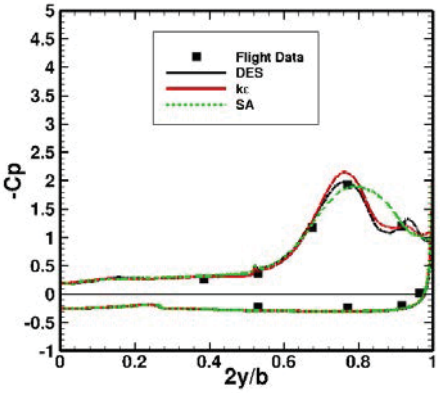

(f) FS 300

Figure 9. Surface Pressure Distributions of Flight Data, RANS kε and SA Turbulence Models Results, (Grid-1), with Time Averaged Results from DES, (GRID-2), on the Medium Grid. ($M_\infty = 0.242$, $\alpha = 19.84°$, $Rn = 32.2 \times 10^6$).

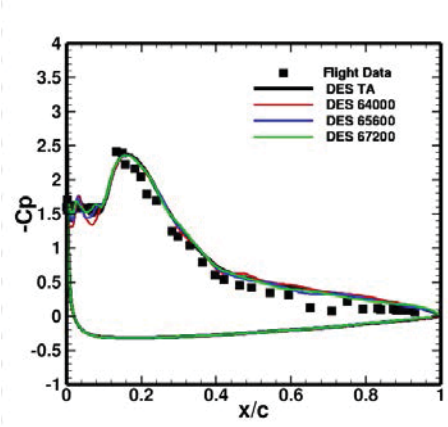

(a) BL 70

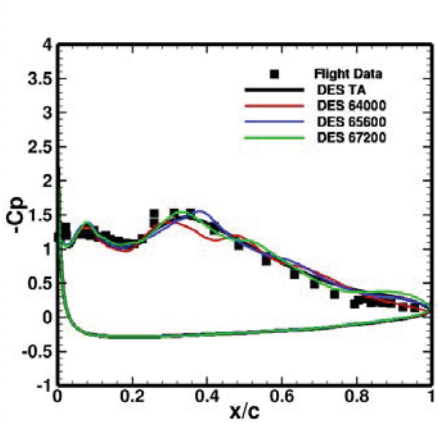

(b) BL 95

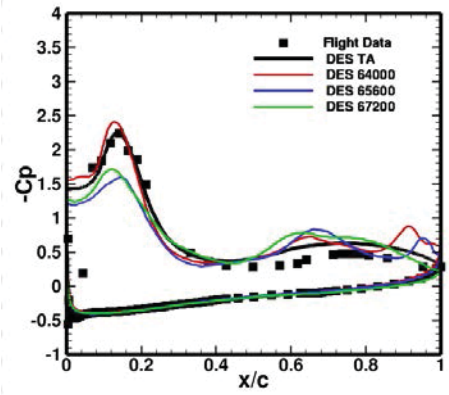

(c) BL 153.5

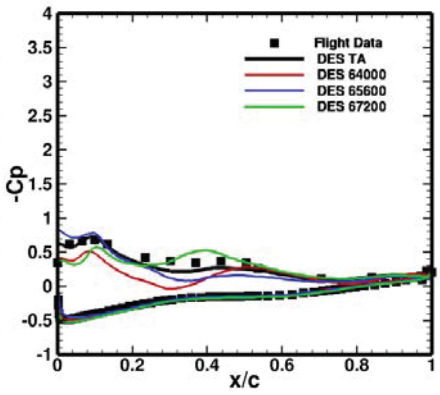

(d) BL 184.5

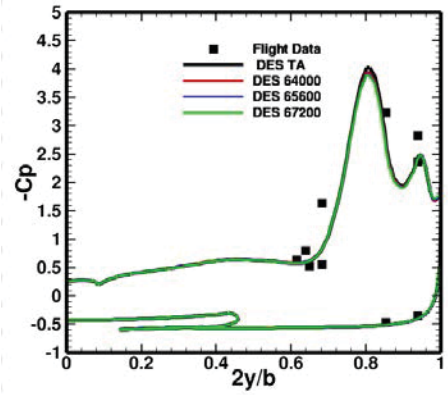

(e) FS 185

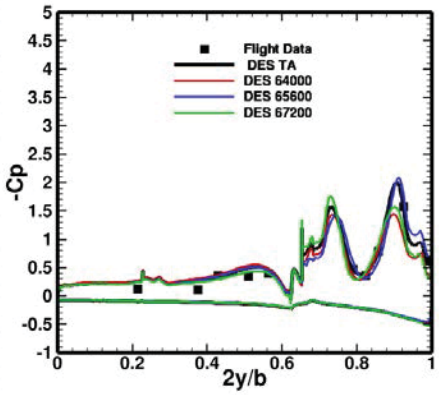

(f) FS 450

Figure 10. Comparison between flight data surface pressure distributions and DES snapshot and time averaged results on medium Grid, (Grid-2).
(M_∞ = 0.242, α = 19.84°, Rn = 32.2 X 10^6).

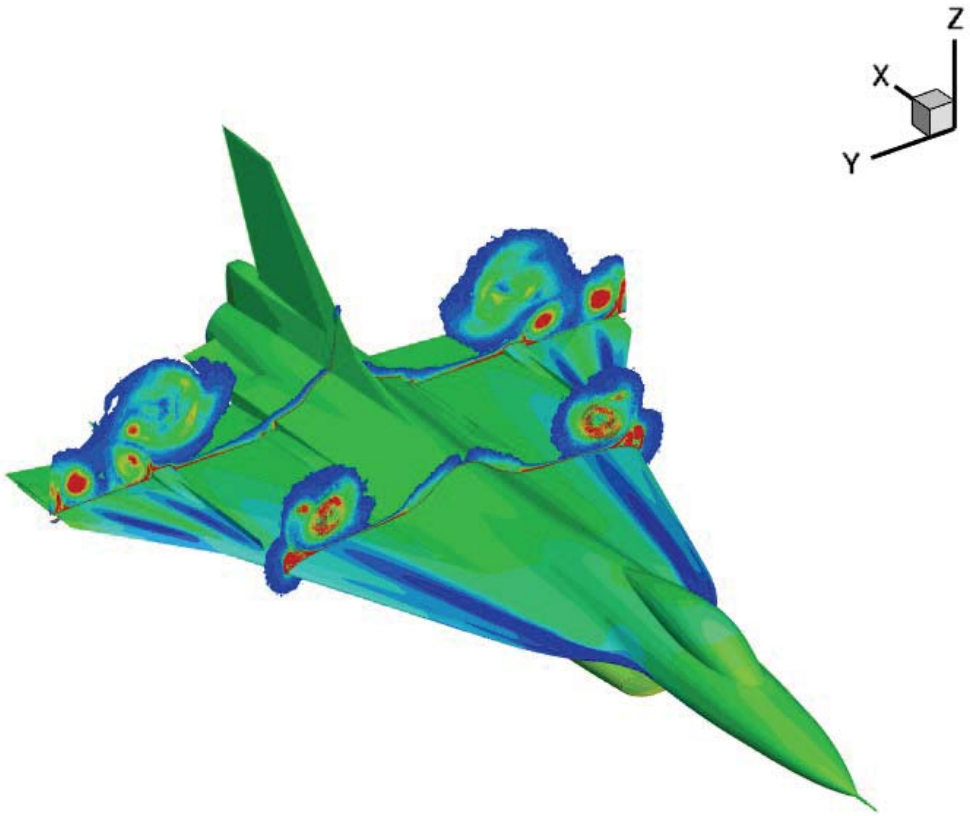

Figure 11. Vortex structure superimposed on the surface pressure for FC 25. (M_∞ = 0.242, α = 19.84°, Rn = 32.2 X 10^6, DES results).

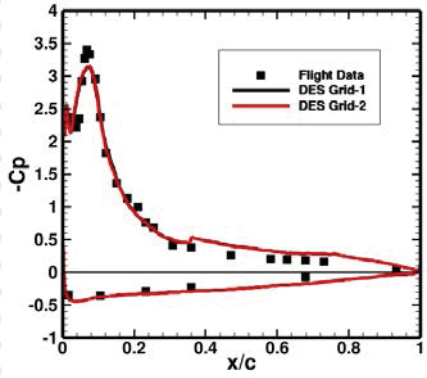

(a) BL 55

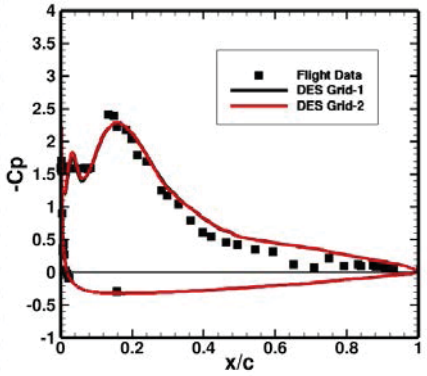

(b) BL 70

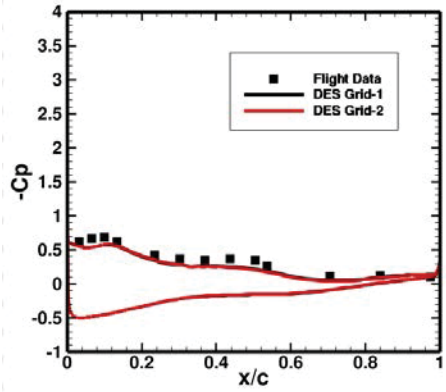

(c) BL 184.5

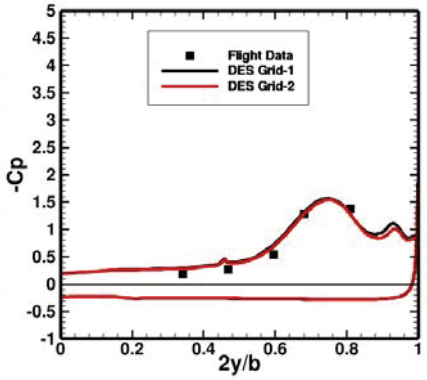

(d) FS 337.5

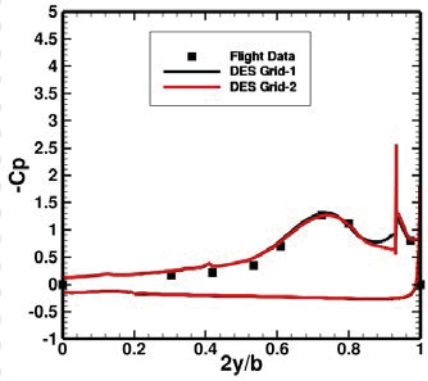

(e) FS 375

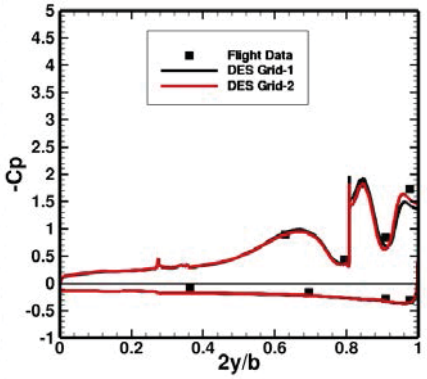

(f) FS 407.5

Figure 12. Comparison between flight data surface pressure distributions and DES time averaged results on Gird-1 and Grid-2.
(M_∞ = 0.242, α = 19.84°, Rn = 32.2 X 10^6).